Chinese Chemical Letters 34 (2023) 107436

Contents lists available at ScienceDirect

Chinese Chemical Letters

journal homepage: www.elsevier.com/locate/cclet

Chlorinated phthalimide polymer donor as ultra-wide bandgap and deep HOMO guest for achieving highly efficient polymer solar cells

Weichao Zhang[a], Jianhua Huang[b], Xiaoyu Lv[c], Ming Zhang[d], Wanru Liu[a], Tianzi Xu[a], Jun Ning[c], Alata Hexig[c], Feng Liu[d], Aiju Xu[a,*], Chuanlang Zhan[a,*]

[a] Inner Mongolia Autonomous University Key Laboratory of Advanced Materials Chemistry and Devices (AMC&DLab), Inner Mongolia Key Laboratory of Green Catalysis, College of Chemistry and Environmental Science, Inner Mongolia Normal University, Huhhot 010022, China
[b] College of Materials Science and Engineering, Huaqiao University, Xiamen 361021, China
[c] Inner Mongolia Key Laboratory of Functional Materials Physics and Chemistry, College of Physics and Electronic Information, Inner Mongolia Normal University, Hohhot 010022, China
[d] School of Chemistry and Chemical Engineering, Center for Advanced Electronic Materials and Devices, Shanghai Jiao Tong University, Shanghai 200240, China

ARTICLE INFO

Article history:
Received 28 February 2022
Revised 29 March 2022
Accepted 11 April 2022
Available online 15 April 2022

Keywords:
Phthalimide polymer donor
Quaternary strategy
Polymer solar cell
Wide bandgap
Fullerene-free

ABSTRACT

Quaternary approach has been receiving more and more attention due to its effectiveness in improving solar cell performance, while synthesis/selection of the fourth component is yet a key issue. Herein, we report a chlorinated phthalimide based donor polymer (namely PhI-Cl) having an ultra-wide bandgap (2.10 eV) and a deep HOMO (−5.58 eV) level. Addition of PhI-Cl as the third component of PM6:Y6 and the fourth of PM6:Y6:$PC_{71}BM$ increases both hole and electron mobilities and gives rise to more balanced charge carriers mobilities. Both the short-circuit current-density and fill-factor are increased and open-circuit voltage is well maintained, delivering 17.0% and 18.1% efficiencies, respectively. These results demonstrate that chlorination on the side thiophene of phthalimide-based donor polymer is a way to make deep HOMO and ultra-wide bandgap donor polymer guest used for highly efficient ternary and quaternary strategies.

Organic solar cells (OSCs) are one of the most attractive next-generation photovoltaic technologies that convert the green and sustainable solar energy into electric power [1–3]. They have attracted increasing interest because of the advantages such as lightweight, mechanical flexibility, and low-cost and large-area printing [4,5]. In recent years, efforts in design of electron-donor and -acceptor materials and innovation in device engineering have led great progress with the power conversion efficiencies (PCEs) over 18% [6–12]. However, simultaneously improvement in open-circuit voltage (V_{oc}) [13], short-circuit current (J_{sc}) [14,15] and fill factor (FF) [16–18] is yet challenging, due to morphological and electronic structure constraints, leading to performance trade-offs. In recent years, ternary strategies have made great progress in the field of OSCs. Introduction of the third components into host binary blended material systems can either broaden light absorption, align energy levels or improve film-morphology, resulting in improved charge dynamics and transportation and increased device stability [19–29]. Nevertheless, the ternary strategies are limited in improving solar cell performance, for examples, due to (1) that the introduction of a single narrower bandgap (E_g^{opt}) generally accompanies with a decrease in V_{oc} and normally a negative influence in blend morphology [30], or (2) that the introduction of a single third component can improve blended structures but without pronounced influences on photocurrent or voltage [31], or (3) that the employment of a single nonfullerene acceptor guest with its LUMO level higher than that of the host can lead to the increase in V_{oc} and normally also in FF, while rarely in J_{sc} [32–36].

Relative to the ternary approaches, the quaternary strategies that allow to introduce more than one extra component into the active layer are solutions to these issues [37–42]. Because of the inclusion of additional two components in the active layer, the quaternary strategy allows us to judiciously select or design two extra components to introduce more photon-to-electron conversion mechanisms. In comparison, this is difficult to be achieved by adding only one component in the ternary strategies [40,43]. For examples, Ma *et al.* [43] selected PBDB-T and ITIC as the third and fourth components of PTB7-Th:FOIC to increase J_{sc} and FF both. Yan *et al.* [44] used PTQ10 and $PC_{71}BM$ as the two extra com-

* Corresponding authors.
E-mail addresses: xuaj@imnu.edu.cn (A. Xu), clzhan@iccas.ac.cn (C. Zhan).

https://doi.org/10.1016/j.cclet.2022.04.034
1001-8417/

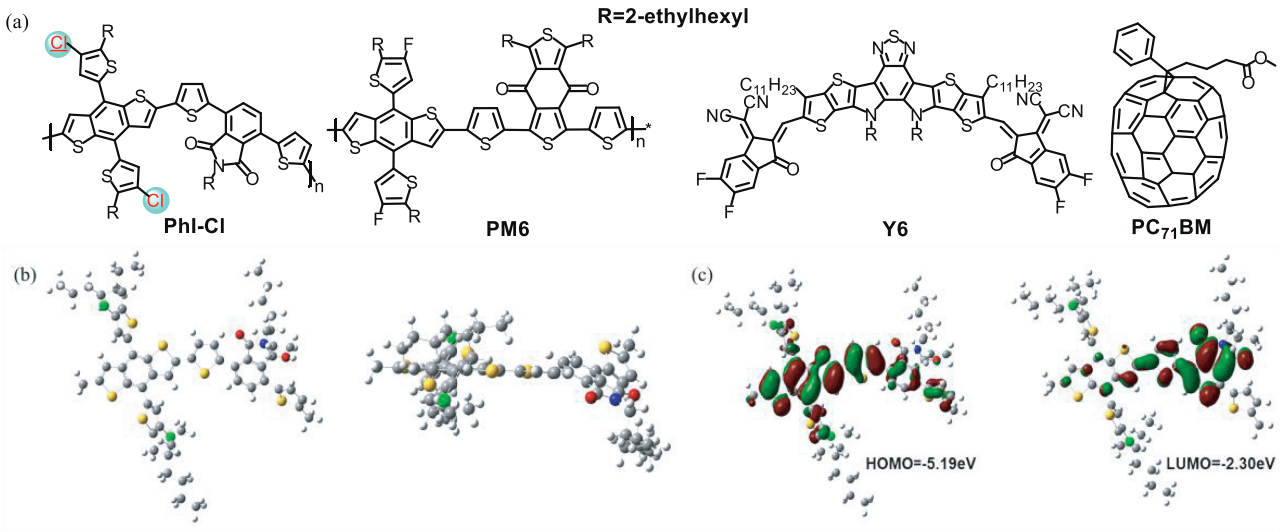

Fig. 1. (a) Molecular structures of the host and guest donor polymers (PhI-Cl and PM6) and the host and guest acceptors (Y6 and $PC_{71}BM$). (b) Top and side views and (c) Distributions of the HOMO and LUMO of the repeating unit BDT-Cl-PhI, optimized using DFT package.

ponents to effectively increase the hole mobility and hence balance the hole and electron mobilities and again suppress charge recombination. Liu *et al.* [10] used PM7 and $PC_{71}BM$ as the quaternary strategy to constitute double cascading energy level alignment to enhance charge splitting and increase carriers mobilities, resulting in simultaneous improvements of J_{sc}, V_{oc} and FF, achieving 18.07% efficiency. We used IDIC and $PC_{71}BM$ as the third and the fourth component to increase phase crystallinity and again increase the phase purity, and reduce the nonradiative energy loss, giving rise to solar cell performance simultaneous increase, obtaining over 17% efficiency [45].

Normally, narrower bandgap polymer donors have been selected as the guest components to achieve absorption-complementary systems so as to enhance the solar light capturing. Recently, we reported a unique case in which we turned to consider using ultra-wide bandgap polymers to increase absorption of the 300-500 nm light. In this case we synthesized two phthalimide based polymers, *e.g.*, PhI-Th and PhI-Se [46,47] as the guest components. Their bandgaps were around 2.0 eV. Use of selnophene rather than thiophene as the π-bridge enabled downshifting the polymers' HOMO levels, being lower than the HOMO level of PM6. This is helpful to maintain or even increase the V_{oc}. The most interesting is that the PhI-Se enabled to selectively tune the fluorinated Y6 [48] phase ordering, which increased electron mobility. Again, PhI-Se formed individual phase other than PM6, leading to increased photocurrent. Taken together, PhI-Se displayed advantages such as (1) ability to selectively tune the fluorinated Y6 phase ordering, (2) ability to form individual phase, and (3) downshifted HOMO level. Synergy of these advantages resulted in a simultaneous increase in solar cell performance. Recent studies have indicated that chlorination, for example, on the side-thiophenes of polymer donors [49–53] such as PM7 [49] or on the end-groups of nonfullerene small-molecule acceptors [54–58] enabled to downshift the energy levels of the Frontier molecular orbitals. Inspired by this, we in this work turn to chlorinate the phthalimide polymer to lower the HOMO energy level and report a new ultra-wide bandgap phthalimide polymer donor guest (PhI-Cl, Fig. 1a). With the chlorination, the HOMO energy is down to −5.58 eV, a little lower than the HOMO level of the host polymer PM6, and the LUMO level is maintained on −2.85 eV. The bandgap is 2.10 eV. Both PhI-Cl and PM6 shared similar fused-ring cores, thus maintaining good compatibility. We introduce PhI-Cl as the additive of PM6:Y6 and further the fourth component of the PM6:Y6:$PC_{71}BM$. First, the deeper HOMO level of PhI-Cl than that of PM6 helps to increase V_{oc}. Second, the compatibility between PhI-Cl and PM6 allows tunability on blended morphology, leading to possibility in increasing charge transportation, and hence, photocurrent generation. Practically, the use of PhI-Cl as the fourth component simultaneously increases both J_{sc} and V_{oc} with maintaining the device FF and thus resulting in 18.13% efficiency, which is one of the top values achieved from quaternary approaches.

We conducted density functional theory (DFT) (Gaussian 09 software, B3LYP) to predict the energy levels and electronic nature of PhI-Cl. The results are given in Figs. 1b and c. Here, one repeating unit, namely BDT-Cl-PhI, was selected to represent the polymer for simulations. The backbone shows slight distortion (Fig. S1 in Supporting information). The dihedral angles between BDT and thiophene, between thiophene and PhI, and between BDT and PhI are about 3°, 32°/28° and 26°, respectively. The HOMO was mainly distributed on BDT-thiophene part, extending to the PhI unit, while the LUMO was mainly observed on the PhI unit. The predicted HOMO and LUMO are a little displaced, which is consistent with the weak electron-withdrawing ability of phthalimide unit, leading to weak intramolecular charge transfer and ultra-wide bandgap.

Fig. 2a shows the absorption profiles of PM6, PhI-Cl, Y6, $PC_{71}BM$ used in this study. The absorption of PhI-Cl is blue-shifted in comparison to that of PM6, covering the 300-600 nm region. The absorption spectra of PhI-Se, PM6 and Y6 are complementary and cover 300–950 nm region. From the cyclic voltametry (CV) measurement (Fig. S2 in Supporting information), the HOMO and LUMO energy levels of PhI-Cl were estimated to −5.58 eV and −2.85 eV, respectively. Fig. 2b displays the energy levels diagram of the four materials. The HOMO level of PhI-Cl is about 0.04 eV downshifted in comparison to that of PM6 and about 0.04 eV higher than the HOMO of Y6, forming aligned energy levels.

The photovoltaic properties of using PhI-Cl as the third additive of PM6:Y6 and the forth component of PM6:Y6:$PC_{71}BM$ were investigated by fabricating normal structure devices. The electron-transporting layer (ETL) material was PFN-Br or PDINO. First, the opyimizations were conducted with PDINO as the ETL material. The best ratio of the four active layer materials was PhI-Cl:PM6:Y6:$PC_{71}BM$ = 0.1:1:1.2:0.1. The optimizations are collected in Table S1 (Supporting information). With PDINO as the

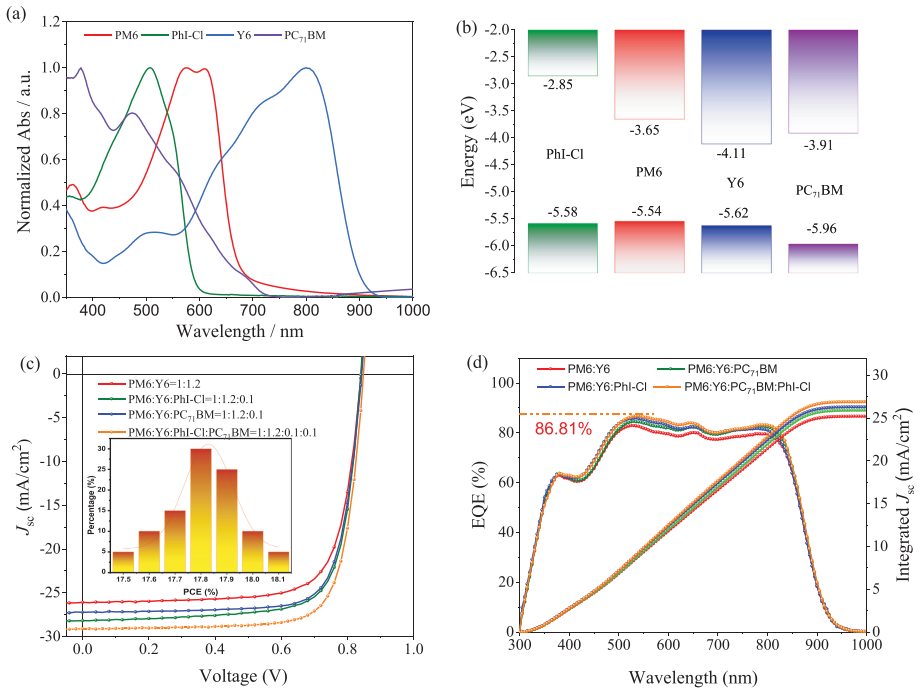

Fig. 2. (a) Film absorption spectra and (b) energy levels of donor polymer (PM6) and guest polymer (PhI-Cl), the host (Y6) and guest ($PC_{71}BM$) acceptors. (c) *J–V* curves (d) EQE curves of the optimized binary, ternary and quaternary devices.

Table 1
The photovoltaic data of binary, ternary, and quaternary devices. All data were obtained under illumination of AM 1.5G (100 mW/cm^2) light source.

Active layer	V_{oc} [a] (V)	J_{sc} [a] (mA/cm^2)	$J_{cacl.}$ [b] (mA/cm^2)	FF [a] (%)	PCE_{ave} [a] (%)
PM6:Y6	0.840 (0.840±0.001)	26.1 (25.8±0.2)	25.2	74.8 (74.34±0.71)	16.4 (16.1±0.19)
PhI-Cl:PM6:Y6	0.840 (0.840±0.002)	26.8 (26.8±0.1)	25.9	75.2 (74.5±0.55)	17.0 (16.8±0.16)
PM6:Y6:$PC_{71}BM$	0.845 (0.843±0.002)	27.2 (27.1±0.3)	26.3	76.5 (76.34±0.31)	17.6 (17.3±0.21)
PhI-Cl:PM6:Y6:$PC_{71}BM$	0.848 (0.844±0.002)	27.7 (27.8±0.1)	27.0	77.1 (76.55±0.40)	18.1 (18.0±0.09)

[a] The average values were obtained from 20 devices.
[b] Obtained from the integration of the EQE spectrum.

ETL, a PCE of 15.95% and a V_{oc} of 0.855 V were obtained from the PM6:Y6 based best device (Table S1). Higher V_{oc} of 0.906 V was obtained from the PhI-Cl:Y6 binary solar cell (Table S1). Adding PhI-Cl as the third component of PM6:Y6, the best performance were observed as the content of PhI-Cl:PM6 was 0.1:1. A PCE of 17.19% was obtained. Both of the V_{oc} and FF were a little increased and the J_{sc} was increased fom 24.71 mA/cm^2 to 26.37 mA/cm^2. The well maintainence of the V_{oc} (0.863 V *vs.* 0.855 V) was due to the deep HOMO level of PhI-Cl in comparison to the HOMO of PM6 (Fig. 2b). When adding 0.1 content of $PC_{71}BM$ into the PhI-Cl:PM6:Y6 (0.1:1:1.2), the solar cell performance was all increased, affording a PCE of 17.72%. This is in accordance with the reproted results in which the addition of PCBM can result in simultaneous increase in solar cell performance [59–61]. When using PFN-Br as the ETL material, a PCE of 16.39% (Table 1) was obtained from the PM6:Y6 binary device. The J_{sc} was 26.09 mA/cm^2, the V_{oc} was 0.840 V, and the FF was 74.79%. The performance was close to the reported values [62]. Adding 0.10 of PhI-Cl as the third component (Table S2 in Supporting information), the best device delivered a higher PCE of 16.97% with the J_{sc} increasing to 26.84 mA/cm^2 and the V_{oc} and FF well maintained. Adding PhI-Cl as the forth component of PM6:Y6:$PC_{71}BM$, the solar cell performance is simultaneously increased, affording an impressive PCE of 18.13% with V_{oc} = 0.848 V, J_{sc} = 27.74 mA/cm^2, and FF =77.05%. The integrated J_{sc} values (Table 1) are consistent with the values obtained from the *J-V* curves. For the quaternary device, the highest EQE appears at 540 nm, around 86.81%. Fig. 2c shows the *J–V* curves of the best solar cell devices illuminated under an AM 1.5G 100 mW/cm^2 light source. Fig. 2d gives the external quantum efficiency (EQE) spectrs. Table 1 collects the device performance.

From Fig. 3a, we can see that the J_{sc} values increase from PM6:Y6 to PhI-Cl based ternary and again from PM6:Y6:$PC_{71}BM$ to the quaternary. Consistently, the estimated hole and electron mobilities showed in Fig. 3b increase in the similar trend. The electron and hole mobilities were measured from the dark $J^{0.5}$-*V* data (Fig. S3 in Supporting information), which were obtained from the space-charge-limited current (SCLC) method. The largest electron and hole mobilities ($\mu_e = 8.63\times10^{-4}$ cm^2 V^{-1} s^{-1}, $\mu_h = 7.31\times10^{-4}$ cm^2 V^{-1} s^{-1}) and again the most balanced electron to hole mobilities ($\mu_e/\mu_h = 1.18$) were observed at the optimized weight ratio of PM6:Y6:PhI-Cl:$PC_{71}BM$ = 1:1.2:0.1:0.1. At the same time, as a reference, we also tested PM6:Y6:$PC_{71}BM$=1:1.2:0.1, and the results showed that its electron and hole mobilities (μ_e/μ_h) are 7.65 × 10^{-4}, 6.14×10^{-4} cm^2 V^{-1} s^{-1}. Compared to the mobilities of the 1:1.2 mixed blend of PM6:Y6, larger hole and electron mobilities were observed when mixing PhI-Cl with the PM6:Y6 binary blend: the electron and hole mobilities (μ_e/μ_h) were 6.61 × 10^{-4}, 5.12×10^{-4} cm^2 V^{-1} s^{-1} and 4.25 × 10^{-4}, 3.14×10^{-4} cm^2 V^{-1} s^{-1}, respectively (Fig. 3b). Again, the mobilities became balanced (Fig. 3b). The values of μ_e/μ_h were 1.25, 1.29 and 1.35 for PM6:Y6:$PC_{71}BM$, PM6:Y6:PhI-Cl and PM6:Y6 based blends, respectively. More balanced carrier mobility was realized after adding PhI-Cl as the third or the fourth component, which agreed with the increased FF values.

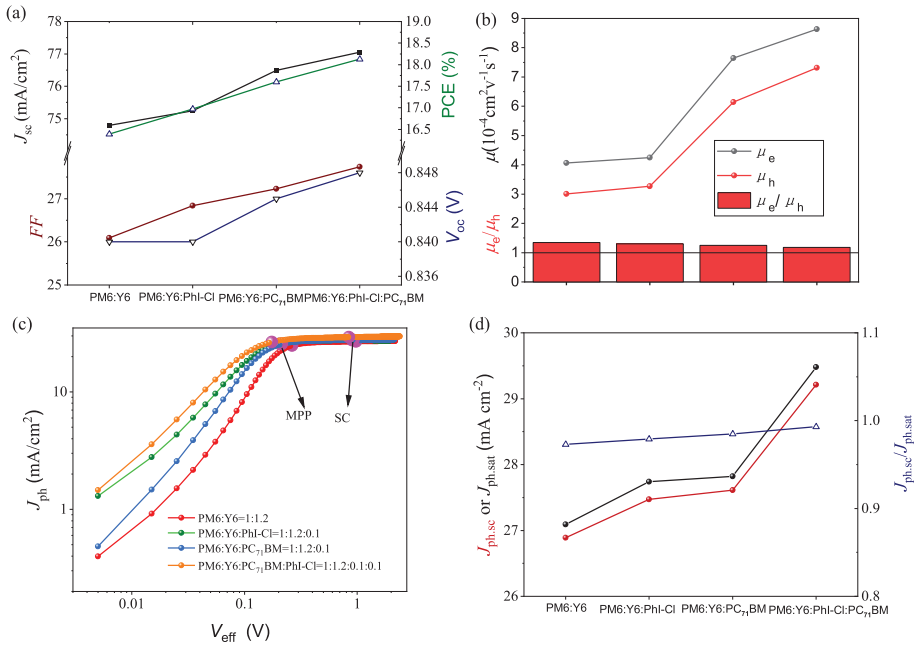

Fig. 3. (a) The plots of the photovoltaic parameters and (b) the hole and electron mobilities (μ_h/μ_e) *versus* the active layer materials, respectively. (c) The J_{ph} *versus* V_{eff} characteristics of the four best solar cell devices and (d) the plots of $J_{ph,sc}$ and $J_{ph,sat}$ *versus* different active layer materials.

In order to see the photocurrent (J_{ph}) generated in the optimal binary, ternary, and quaternary solar cell devices, we measured both the illuminated and dark *J*–*V* curves of the corresponding solar cell devices. Fig. 3c are the plots of J_{ph} as a function of V_{eff}, here, V_{eff} is the effective internal field with $V_{eff} = V_0 - (V_{bias} + J_{ph} \cdot R_S)$, V_{bias} is the applied voltage and V_0 is the voltage when $J_{ph} = 0$ mA/cm^2. The term of $J_{ph} \cdot R_S$ is added to correct the applied bias V_{bias} for the voltage loss occurring over the series resistance [63]. J_{ph} increases at the low V_{eff} range and tends to be saturated around MPP (maximum power point). This trend suggests that the carriers are efficiently transported and collected by the right electrode at a large V_{eff} regime in each solar cell device. To compare the collection of photogenerated charges in binary, ternary and quaternary devices, we calculated the J_{ph} values at the short-circuit ($J_{ph,sc}$), the MPP, and the saturated points ($J_{ph,sat}$) (Table S3 in Supporting information). Fig. 3d shows the plots of $J_{ph,sc}$ (red line) and $J_{ph,sat}$ (black line) versus the active layer materials. Both $J_{ph,sc}$ and $J_{ph,sat}$ are increased with PhI-Cl as the third component of PM6:Y6 and the fourth component of PM6:Y6:PC$_{71}$BM, which agrees with the trend of change in J_{sc} values obtained from these devices. The charge collection efficiencies at the MPP and short-circuit conditions are demonstrated by $J_{ph,MPP}/J_{ph,sat}$ and $J_{ph,sc}/J_{ph,sat}$ (Table S3 in Supporting information). We can see that both the $J_{ph,MPP}/J_{ph,sat}$ and $J_{ph,sc}/J_{ph,sat}$ increase with adding PhI-Cl as the third component of PM6:Y6 and again the fourth component of PM6:Y6:PhI-Cl:PC$_{71}$BM.

To see the recombination of charge carriers at short-circuit and open-circuit conditions, respectively, Figs. 4a and b show the plots of the J_{sc} and V_{oc} as a function of the incident light intensity (P_{light}). From the linear fittings of lnJ_{sc} *vs.* lnP_{light} (Fig. 4a) and V_{oc} *vs.* lnP_{light} (Fig. 4b), α and nkT/q values are obtained (showed in the right figures), respectively. Here, *k*, *T* and *q* are the Boltzmann constant, temperature in Kelvin, and the elementary charge, respectively. The values of α increase from 0.960 to 0.975 and again from 0.977 to 0.985 when PhI-Cl as the third component of PM6:Y6 and again the fourth component of PM6:Y6:PC$_{71}$BM, meaning that the bimolecular recombination at the short-circuit condition can be suppressed when adding PhI-Cl as the extra component. This is consistent with the increase of the device FF. The *n* values are slightly decreased when adding PhI-Cl, meaning that adding PhI-Cl well maintains the monomolecular recombination.

As shown in Fig. S4 (Supporting information), about 40% of the fluorescence spectrum of PhI-Cl is overlapped with the absorption spectrum of PM6, which suggests the possible energy transfer from PhI-Cl to PM6. We therefore fabricated the 0.1:1 blended PhI-Cl:PM6 film and measured the absorption and fluorescence spectra, which are shown in Fig. S4 with the blue solid and dashed lines. Compared with the fluorescence spectra of PhI-Cl and PM6 films, the high-wavelength edge of the fluorescence spectrum of the PhI-Cl:PM6 blend is nearly identical to that of the pure PM6 film. This means that the energy transfer from PhI-Cl to PM6 might be take place. Again, the fluorescent peak of the blend is red-shifted in comparison to that of PM6, suggesting that adding PhI-Cl might induce a change in the packing of PM6 molecules. This is supported by comparison of the absorption spectra of the pure PM6 and the blend: compared with the absorbance at 611 nm, the absorbance at 574 nm is relatively increased after the PM6 is mixed with 0.1 PhI-Cl.

The film morphologies of the binary, ternary and quaternary solar cell blend films were first investigated *via* transmission electron microscopy (TEM) and atomic force microscopy (AFM) height and phase techniques (Fig. S5 in Supporting information). In TEM images (Figs. S5a–d), phase-separated nanoscaled fibril networks are seen for the four solar cell film blends. After adding PhI-Cl as the third component of PM6:Y6 and as the fourth component of PM6:Y6:PC$_{71}$BM, the phase-separated white and dark domains become more contracted. Relatively larger white and dark domains are seen, which is consistent with the increased charge mobilities and the increased short-circuit current. The AFM height (Figs. S5e-h) and phase (Figs. S5i-l) images also demonstrate the fine fibril networks on the surfaces of the binary, the two ternary and the quaternary blends. The root-mean-square (RMS) roughness is 0.77 nm for the PM6:Y6 (1:1.2) binary blend and increases to 1.30 nm after adding PhI-Cl. Again, the RMS value also increases from 0.82 nm to 1.38 nm after adding PhI-Cl as the fourth component of PM6:Y6:PC$_{71}$BM.

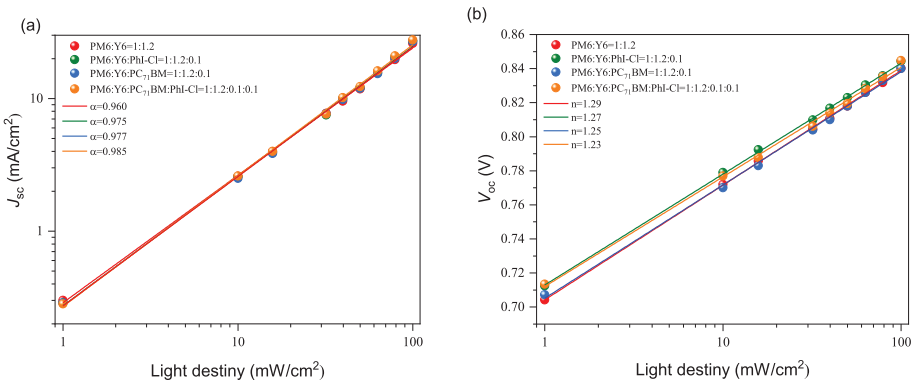

Fig. 4. (a) Plots of J_{sc} *vs.* light intensity and (b) V_{oc} *vs.* light intensity for the four best solar cell devices.

The structures of the four solar cell blend films were further studied with 2-D graze-incidence wide-angle X-ray scattering (GIWAXS). Fig. S6 (Supporting information) shows the GIWAXS data of the binary, the two ternary and quaternary blends plus the pure PhI-Cl film. The PhI-Cl tends to adapt the face-on orientation. When adding PhI-Cl as the extra component, the perfect face-on orientation of the PM6:Y6 blend are well kept, which can be explained with the structural similarity of the PhI-Cl and PM6 backbones. The coherent crystalline length (CCL) values of the π–π stacking are estimated to be 18.03 nm and 17.55 nm after the addition of 0.1 PhI-Cl. For the lamellar stacking of the sidechains, the structural information is reflected from the 0.28 $Å^{-1}$ diffraction signal, from which the calculated CCL values are increased from 30 nm for the PM6:Y6 binary blend to 37 nm for the PhI-Cl ternary blend and then from 33 nm for the PM6:Y6:PC_{71}BM blend to 41 nm for the quaternary blend. This reflects that the aggregated structure of the donor phases is more ordered after adding PhI-Cl as the extra component, which is consistent with the increased hole mobilities.

In summary, we report a chlorinated phthalimide based donor polymer in which the side thiophene units were chlorinated to form an ultra-wide bandgap and deep HOMO level donor (*e.g.*, PhI-Cl). PhI-Cl was used as the guests for fabricating highly efficient ternary and quaternary organic solar cells. When adding PhI-Cl as the third component of PM6:Y6 and the fourth component of PM6:Y6:PC_{71}BM, respectively, both the hole and electron mobilities were increased and again became more balanced, resulting in simultaneous increase in solar cell performance and affording 17% and 18.1% efficiencies ternary and quaternary solar cells. Addition of PhI-Cl increased the lamellar packing ordering and formed larger donor and acceptor phase domains, again decreasing the bimolecular recombination at the short-circuit condition. These results indicate that phthalimide polymers can be efficient guest components when judiciously designing their side chains and HOMO levels.

Declaration of competing interest

There are no conflicts to declare.

Acknowledgments

C. Zhan gratefully acknowledges the financial support of the Department of Science and Technology of Inner Mongolia (No. 2020GG0192), Grassland Talents (No. CYYC10031) and Inner Mongolia Normal University (No. 112/1004031962). A. Xu acknowledges the financial support of Collaborative Innovation Center for Water Environment Security of Inner Mongolia Autonomous Region, China (No. XTCX003).

Supplementary materials

Supplementary material associated with this article can be found, in the online version, at doi:10.1016/j.cclet.2022.04.034.

References

[1] P. Cheng, G. Li, X. Zhan, Y Yang, Nat. Photon. 12 (2018) 131–142.
[2] J. Zhang, H.S. Tan, X. Guo, A Facchetti, H Yan, Nat. Energy 3 (2018) 720–731.
[3] D. Baran, T. Kirchartz, S. Wheeler, et al., Energ. Environ. Sci. 9 (2016) 3783–3793.
[4] F.C. Krebs, N. Espinosa, M. Hösel, R.R. Søndergaard, M. Jørgensen, Adv. Mater. 26 (2014) 29–39.
[5] Y. Cui, Y. Wang, J. Bergqvist, et al., Nat. Energy 4 (2019) 768–775.
[6] L. Zhan, S. Li, X. Xia, et al., Adv. Mater. 33 (2021) 2007231.
[7] C. Li, J. Zhou, J. Song, et al., Nat. Energy 6 (2021) 605–631.
[8] S. Chen, L. Feng, T. Jia, et al., Sci. China Chem. 64 (2021) 1–8.
[9] F. Liu, L. Zhou, W. Liu, et al., Adv. Mater. 33 (2021) 2100803.
[10] M. Zhang, L. Zhu, G. Zhou, T. Hao, F. Liu, Nat. Commum. 12 (2021) 1–10.
[11] Y. Li, Y. Cai, Y. Xie, et al., Energ. Environ. Sci. 14 (2021) 5009–5016.
[12] T. Zhang, C. An, P. Bi, et al., Adv. Energy Mater. 11 (2021) 2101705.
[13] Y. Liu, Z. Zhang, S. Feng, et al., J. Am. Chem. Soc. 139 (2017) 3356–3359.
[14] L. Zhan, S. Li, H. Zhang, et al., Adv. Sci. 5 (2018) 1800755.
[15] X. Ma, Y. Mi, F. Zhang, et al., Adv. Energy Mater. 8 (2018) 1702854.
[16] M. Zhang, W. Gao, F. Zhang, et al., Energ. Environ. Sci. 11 (2018) 841–849.
[17] Z. Zhou, S. Xu, J. Song, et al., Nat. Energy 3 (2018) 952–959.
[18] Z. Zheng, Q. Hu, S. Zhang, et al., Adv. Mater. 30 (2018) 1801801.
[19] Y. Xie, F. Yang, Y. Li, et al., Adv. Mater. 30 (2018) 1803045.
[20] H. Fu, Z. Wang, Y. Sun, Solar RRL 2 (2018) 1700158.
[21] D. Landerer, A. Mertens, D. Freis, et al., Npj Flexible Electr. 1 (2017) 1–8.
[22] Y. Dong, Y. Zou, J. Yuan, et al., Adv. Mater. 31 (2019) 1970371.
[23] J. Wan, L. Zhang, Q. He, et al., Adv. Funct. Mater. 30 (2020) 1909760.
[24] R. Yu, H. Yao, J. Hou, Adv. Energy Mater. 8 (2018) 1702814.
[25] K. Feng, Z. Wu, M. Su, et al., Adv. Funct. Mater. 31 (2021) 2008494.
[26] Z.S. Wang, X. Ren, X. Xu, et al., Nano Energy 51 (2018) 206–215.
[27] L. Xiao, H. Mao, Z. Li, C. Yan, Y. Liu, ACS Appl. Mater. Interfaces 12 (2020) 16387–16393.
[28] J.W. Lee, C. Sun, B.S. Ma, et al., Adv. Energy Mater. 11 (2021) 2003367.
[29] D. Li, X. Chen, J. Cai, et al., Sci. China Chem. 63 (2020) 1–8.
[30] H. Yao, Y. Cui, R. Yu, et al., Angew. Chem. Int. Ed. 129 (2017) 3091–3095.
[31] Q. An, F. Zhang, L. Li, W. Jian, Z. Deng, ACS Appl. Mater. Interfaces 7 (2015) 3691–3698.
[32] Y. Chang, T.K. Lau, M.A. Pan, et al., Mater. Horiz. 6 (2019) 2094–2102.
[33] K. Li, Y. Wu, Y. Tang, et al., Adv. Energy Mater. 9 (2019) 1901728.
[34] Y. Cui, H. Yao, J. Zhang, et al., Nat. Commum. 10 (2019) 1–8.
[35] J. Song, C. Li, L. Zhu, et al., Adv. Mater. 31 (2019) 1905645.
[36] V.K. Karapala, T.W. Chen, K.J. Ma, et al., ACS Appl. Energy Mater. 4 (2021) 2847–2855.
[37] W. Li, D. Yan, F. Liu, et al., Sci. China. Chem. 61 (2018) 1609–1618.
[38] D. Yan, J. Xin, W. Li, et al., ACS Appl. Mater. Interfaces 11 (2018) 766–773.
[39] F. Shen, D. Yan, W. Li, et al., Mater. Chem. Front. 3 (2019) 301–307.
[40] L. Liu, H. Chen, W. Chen, F. He, J. Mater. Chem. A 7 (2019) 7815–7822.
[41] Z. Bi, Q. Zhu, X. Xu, et al., Adv. Funct. Mater. 29 (2019) 1806804.
[42] W. Li, W. Liu, X. Zhang, et al., Mac. Rapid Commun. 40 (2019) 1900353.
[43] W. Li, D. Yan, F. Liu, et al., Sci. China. Chem. 61 (2018) 1609–1618.
[44] L. Arunagiri, Z. Peng, X. Zou, et al., Joule 4 (2020) 1790–1805.
[45] K. Li, Y. Wu, X. Li, H. Fu, C. Zhan, Sci. China. Chem. 63 (2020) 490–496.
[46] H. Meng, Y. Li, B. Pang, et al., J. Mater. Chem. C 7 (2019) 8442–8449.
[47] W. Zhang, J. Huang, J. Xu, et al., Adv. Energy Mater. 10 (2020) 2001436.
[48] J. Yuan, Y. Zhang, L. Zhou, et al., Joule 3 (2019) 1140–1151.
[49] S. Zhang, Y. Qin, J. Zhu, J. Hou, Adv. Mater. 30 (2018) 1800868.
[50] A. Zeng, X. Ma, M. Pan, et al., Adv. Energy Mater. 31 (2021) 2102413.
[51] Y. Dong, H. Yang, Y. Wu, et al., J. Mater. Chem. A 7 (2019) 2261–2267.

[52] M. Zhang, X. Xu, L. Yu, Peng Q, J. Power Sources 499 (2021) 229961.
[53] Y. Zhao, L. Yu, Y. Li, et al., J. Mater. Chem. C 9 (2021) 14209–14216.
[54] D. Mo, H. Chen, J. Zhou, et al., J. Mater. Chem. A 8 (2020) 8903–8912.
[55] Y. Li, H. Meng, J. Huang, C. Zhan, ACS Appl. Mater. Interfaces 12 (2020) 50541–50549.
[56] B. Zhao, H. Wu, J. Su, et al., ACS Appl. Energy Mater. 4 (2021) 12974–12981.
[57] C. He, Y. Li, S. Li, et al., ACS Appl. Mater. Interfaces 12 (2020) 16700–16706.
[58] S. Wan, Y. Ma, D. Cai, et al., Adv. Funct. Mater. 31 (2021) 2010436.
[59] M.A. Pan, T.K. Lau, Y. Tang, et al., J. Mater. Chem. A 7 (2019) 20713–20722.
[60] R. Yu, H. Yao, Y. Cui, et al., Adv. Mater. 31 (2019) 1902302.
[61] T. Yan, W. Song, J. Huang, et al., Adv. Mater. 31 (2019) 1902210.
[62] L. Zhu, M. Zhang, G. Zhou, et al., Adv. Energy Mater. 10 (2020) 1904234.
[63] J. Vollbrecht, V.V. Brus, S.J. Ko, et al., Adv. Energy Mater. 9 (2019) 1901438.